Millimeter-sized magnetic domains in perpendicularly magnetized ferrimagnetic Mn_4N thin film grown on $SrTiO_3$

Toshiki Gushi[1,2], Laurent Vila [2], Olivier Fruchart[2], Alain Marty[2], Stefania Pizzini[3], Jan Vogel[3], Fumiya Takata[1], Akihito Anzai[1], Kaoru Toko[1], Takashi Suemasu[1,a)], and Jean-Philippe Attané[2,b)]

[1] *Institute of Applied Physics, Graduate School of Pure and Applied Sciences, University of Tsukuba, Tsukuba, Ibaraki 305-8573, Japan*

[2] *Univ. Grenoble Alpes, CEA, CNRS, INAC-Spintec, 38000 Grenoble, France*

[3] *Univ. Grenoble Alpes, CNRS, Institut NEEL, 38000 Grenoble, France*

a) Electronic mail: suemasu@bk.tsukuba.ac.jp

b) Electronic mail: jean-philippe.attane@cea.fr

Abstract

The magnetic properties of 10-nm-thick ferrimagnetic Mn_4N epitaxial films deposited on MgO(001) and $SrTiO_3$(001) substrates have been characterized by magneto-transport measurements, magnetic force microscopy and Kerr microscopy. The hysteresis loop of Mn_4N/MgO exhibits a moderate remanence (M_r/M_S = 0.71), while that of Mn_4N/$SrTiO_3$

sample displays a sharp switching and a full remanence (M_r/M_S = 1.0) with a high perpendicular anisotropy field of 4 T. Magnetic domains in Mn_4N/MgO are irregular and submicronic, while those in $Mn_4N/SrTiO_3$ are millimeter-sized and separated by smooth domain walls. This reflects a higher crystalline quality, which can be attributed to the smaller lattice mismatch between the Mn_4N layer and the $SrTiO_3$ substrate. With a low magnetization, a large perpendicular anisotropy and smooth domain walls, $Mn_4N/SrTiO_3$ is a promising system for current-induced domain wall motion.

Text

Current induced domain wall motion (CIDWM) is actively studied theoretically[1,2,3,4] and experimentally[5,6,7], because it raises new questions concerning the interplay between spin and charge currents, and in order to prospect for new spintronic devices such as non-volatile memories based on domain wall (DW) motion[8]. During one decade, spin-transfer torques from the current flowing within the magnetic material was the only physical effect known to allow domain wall motion. The discovery of spin-orbit torques (SOT) in multilayers systems[9,10)], brought more versatility and greater efficiency. This largely shifted the focus of the community towards spinorbitronics[11].

Concerning the choice of materials, simulation and experiment[12,13] show that in perpendicularly magnetized ferrimagnets the critical current densities required to induce domain-wall motion by spin transfer torque or by SOT is greatly reduced, because of the low value of the magnetization. Thus, the combination of both STT/SOT and ferrimagnets is a very attracting pathway for creating spintronics devices based on DW motion or on nanomagnet switching, for which minimizing the operating currents allows obtaining a lower energy consumption and areal footprint[14]. For example, Je *et al*. reported the enhancement of the SOT efficiency in a CoTb/Pt stack with a compensated alloy composition, and obtained a high SOT efficiency (3.7×10^{-13} Tm^2/A[15)], three times larger than that of Ta/CoTb[16] and five times larger than that of Pt/Co/AlO_x[17].

Until now, most perpendicular ferrimagnetic materials used for DW motion experiments are rare-earth based, with potential concerns about material criticality in the context of the rising demand for these elements. Anti-perovskite-type nitrides with 3*d* transition metals could be interesting rare-earth free candidates for replacement. Among them, Mn_4N has a high Curie temperature T_C of 740 K[18], a small spontaneous magnetization M_S (100 kA/m) and a strong perpendicular magnetic anisotropy (PMA), with $\mu_0 H_K$ values over 2.5 T[19,20]. Mn_4N samples with PMA have been successfully grown on several kinds of substrates, such as glass[21], Si(100)[22,23], SiC[24], MgO[19,20,25,26] and $SrTiO_3$(STO)[19,20].

In the following, we study 10-nm-thick Mn_4N epitaxial thin films deposited on MgO(001) and STO(001) substrates by molecular beam epitaxy (MBE). Using structural characterizations, magneto-transport measurements, vibrating sample magnetometer (VSM) and magnetic imaging techniques, we study the influence of the substrate on the magnetic properties, showing that the use of STO substrates allows obtaining astonishing DW properties, with seemingly very few pinning and a spontaneous domain size in the millimeter range.

SiO_2(3 nm)/Mn_4N(10 nm) layers have been deposited on MgO(001) and STO(001) substrates at 450 °C, using a MBE system with an ion-pump (10^{-7} Pa), equipped with a high-temperature Knudsen cell for Mn and a radio-frequency (RF) N_2 plasma[19,20]. To prevent oxidation, the samples have been capped with 3-nm-thick SiO_2 layers.

The crystalline quality of the Mn_4N layer has been characterized by 20-kV reflection high-energy electron diffraction (RHEED) and x-ray diffraction (XRD) with Cu K_α radiation. Figure 1 presents the (a), (b) out-of-plane ($\omega - 2\theta$) and (c), (d) in-plane ($\phi - 2\theta_\chi$) XRD with RHEED patterns of the grown Mn_4N layers on MgO and STO substrates, respectively. ω-scan rocking curves are shown in the same figure for (e) Mn_4N 002 on MgO, (f) Mn_4N 004 on STO.

For Mn_4N/MgO, the XRD peaks of the film and substrate are well split, which allows extracting information on the magnetic layer. On the contrary, the diffraction peak of Mn_4N 002 is so close to STO 002 that we need to analyze the higher-order Mn_4N 004 rocking curves to separate each peak. These rocking curves have been fitted by a Lorentzian function.

A common feature of both systems is the observation of streaky RHEED patterns and of XRD peaks of *c*-axis-oriented Mn_4N such as 001 or 002. Both these observations are proof of the epitaxial growth of the Mn_4N film. However, the width of the rocking curves are obviously different, indicating that Mn_4N films are much better textured when deposited on STO rather than on MgO. This result is similar to what has been observed for Fe_4N film[27]. The superlattice reflections in the RHEED pattern, together with the 001 peak in the XRD pattern, indicate the good long-range ordering and the presence of the N atom at the body center of the fcc-Mn lattice. X-ray reflectometry provides also an accurate measurement of the magnetic films thicknesses, giving 8.8 nm for the Mn_4N/MgO sample and 9.4 nm for the Mn_4N/STO sample.

Magneto-transport properties, such as the magnon-magnetoresistance (MMR) [28,29] and the extraordinary Hall effect (EHE), have been measured by the Van der Pauw method for Mn_4N blanket layers at room temperature, using lock-in techniques at 210 Hz. The resistivity at room temperature is 187 μΩ.cm for the Mn_4N/MgO sample, and 181 μΩ.cm for the Mn_4N/STO sample. As shown in Figs. 2(a) and (b), the magnetoresistance is dominated by the MMR. This indicates the strong uniaxial magnetization anisotropy.

Figures 2 (c) and (d) show the hysteresis loops measured by EHE. The EHE angle ρ_{xy}/ρ_{xx} is high, of –2%, in line with previous reports on Mn_4N,[30,31]. While the Mn_4N/MgO sample shows a smooth hysteresis loop, the magnetization of the Mn_4N/STO sample switches very sharply, with a full remanence at zero field. Despite these differences, it is striking that the spontaneous magnetization and all transport quantities are very similar for the two systems, which shows that the intrinsic materials are very similar. Based on the above-discussed structural characterization, we believe that the structural disorder is responsible for the higher coercivity and slanted loop of Mn_4N/MgO samples.

Figures 2(e) and 2(f) present the out-of-plane and in-plane magnetization curves, obtained by VSM-SQUID up to 4 and 6 T, respectively, of Mn_4N/MgO and Mn_4N/STO. From out-of-plane

M-H curves we found M_S of Mn_4N/MgO and Mn_4N/STO to be 118 and 105 kA/m, respectively. From in-plane loop of Mn_4N/STO, the anisotropy field H_K was estimated to be 4 T. The uniaxial anisotropy K_u was calculated to be 1.1×10^5 J/m^3, from the integration of the area enclosed between the in-plane and out-of-plane magnetization curves and taking into account the demagnetization energy.

Let us discuss now the magnetic domain configuration in Mn_4N thin films. The theoretical equilibrium domain size in Mn_4N layers results from the balance between dipolar energy and DW energy. With M_S=105 kA/m, K_u =110 kJ/m^3, and an exchange stiffness A=15 pJ/m from rough estimation from Curie temperature [32], the DW width is $\sqrt{A/K_u} = 12$ nm. The resulting equilibrium domain size for a 10-nm-thick Mn_4N film, calculated using the analytical model of ref. [33], is 42 km. This indicates that because of the small M_S the effects of the demagnetizing field are negligible, and that in practice the domain size and shape shall be rather determined by DW pinning on extrinsic defects[34].

Let us examine the domain pattern in Mn_4N layers on MgO and STO substrates. For each kind of sample, the magnetic domain configuration has been observed by magnetic force microscopy (MFM) and/or magneto-optical Kerr effect (MOKE) microscopy, depending on the typical length scale found for the magnetic domains. The mean domain period d_p was estimated from 2D fast Fourier transformation method in the same way as Ref. [35]. The observation has

been performed both for the as-deposited state and after partial magnetization reversal at the coercive field. Figures 3 (a) and (b) ~~shows~~ show the magnetic domain configuration before any application of magnetic field, which is a state often considered to be close to the equilibrium state. In Mn_4N/MgO samples, magnetic domains are small (d_p = 0.28 μm), far below the theoretical equilibrium width. The irregular shape of the DWs is characteristic of a strong disorder[34]. On the contrary, the magnetic domain size in the Mn_4N/STO sample is 2 orders of magnitude larger, with d_p as large as 20 μm, and with smooth magnetic DWs possessing longer correlation length. Though this value is much smaller than the theoretical equilibrium width, this indicates a much lower influence of the extrinsic disorder, nonetheless a value comparable with that of ultrathin CoFeB/MgO and Pt/Co system, 14 and 6.5 μm obtained after thermal demagnetization, respectively[35],[36].

Figure 3(c) shows the Hall signal of Mn_4N/STO during typical partial reversal process. Figure 3 (d) and (e) present the domain configurations of both samples in partially reversed states. In the case of Mn_4N/MgO, the structure of the domains is almost the same as in the as-deposited state, while the domain structure in Mn_4N/STO evolved from a micron-sized configuration to a millimeter-sized one, a value never reported to our best knowledge in any perpendicularly magnetized thin films. There are few nucleation centers in the MOKE images, which suggests that the magnetization switching occurs by a hard nucleation followed by an easy propagation. Note that this hypothesis is consistent with the fact that the hysteresis loop is

square.

The differences between the two systems are striking, both concerning its hysteresis loops, and its domains shapes and sizes. The XRD data and the magnetic properties suggest that these differences arise from the crystalline quality of the samples, which is higher for the Mn_4N/STO samples. The physical origin could be strain relaxation: there is a large lattice misfit $f = (a_{film}-a_{sub})/a_{sub}$ at the Mn_4N/MgO interface (–7.6%), whereas the misfit at the Mn_4N/STO interface is only –0.4%. While the existence of misfit dislocations at Mn_4N/MgO interface has already been observed by transmission electron microscopy[25], other strain-relaxation through-dislocations of micro-grain boundaries are also expected to play a major role in the magnetic behavior. This underlines that the selection of a well-matching substrate is crucial to improve the magnetic properties of Mn_4N layers, and notably its suitability for current-induced DW propagation.

Conclusion

In summary, we showed that the magnetic functional properties of perpendicularly magnetized Mn_4N layer are dramatically improved when replacing MgO substrates by STO substrates. This Mn_4N/STO system exhibits astonishing properties: a giant domain structure, at the millimeter length scale, with full remanence, scarce nucleation and a sharp magnetization switching. These properties, associated to a very small M_S and a large PMA underline the

potential of Mn_4N/STO layers for CIDWM.

ACKNOWLEDGMENTS

This work was supported in part by JSPS Grants-in-Aid for Scientific Research (A) (No. 26249037) and JSPS Fellows (Nos. 16J02879). Magnetization measurements have been performed with the help of Professor H. Yanagihara of the University of Tsukuba, and MFM images thanks to the help of Simon Le Denmat, from Institut Néel. Support from the ANR OISO and LABEX Lanef are also acknowledged.

---

[1] L. Berger, Phys. Rev. B **54**, 9353 (1996).

[2] J. C. Slonczewski, J. Magn. Magn. Mater. **159**, L1 (1996).

[3] G. Tatara and H. Kohno, Phys. Rev. Lett. **92**, 086601 (2004).

[4] Z. Li and and S. Zhang, Phys. Rev. Lett. **92**, 207203 (2004).

[5] N. Vernier, D. A. Allwood, D. Atkinson, M. D. Cooke, and R. P. Cowburn, Europhys. Lett. **65**, 526 (2004).

[6] A. Yamaguchi, T. Ono, S. Nasu, K. Miyake, K. Mibu, and T. Shinjo, Phys. Rev. Lett. **92**, 077205 (2004).

[7] G. S. D. Beach, C. Knutson, C.Nistor, M. Tsoi, and J. L. Erskine, Phys. Rev. Lett. **97**, 057203 (2006).

[8] S. Fukami, T. Suzuki, K. Nagahara, N. Ohshima, Y. Ozaki, S. Saito, R. Nebashi, N. Sakimura, H. Honjo, K. Mori, C. Igarashi, S. Miura, N. Ishiwata and T. Sugibayashi, 2009 Symposium on VLSI Technology. Digest Tech. Pap. 230 (2009).

[9] I. M. Miron, T. Moore, H. Szambolics, L. D. Buda-Prejbeanu, S. Auffret, B. Rodmacq, S. Pizzini, J. Vogel, M. Bonfim, A. Schuhl and G. Gaudin, Nat. Mater. **10**, 419 (2011).

[10] L. Liu, T. Moriyama, D. C. Ralph and R. A. Buhrman, Phys. Rev. Lett. **106**, 036601 (2011).

[11] P. Gambardella and I. M. Miron, Phil. Trans. R. Soc. A **369**, 3175 (2011).

[12] T. Komine, K. Takahashi, A. Ooba and R. Sugita, J. Appl. Phys. **109**, 07D5030 (2011).

[13] D.-T. Ngo, K. Ikeda and H. Awano, Appl. Phys. Express **4**, 093002 (2011).

[14] D. Bang and H. Awano, Appl. Phys. Express **5**, 125201 (2012).

[15] S.-G. Je, J.-C. Rojas-Sanchez, T. H. Pham, P. Vallobra, G. Malinowski, D. Lacour, T. Fache, M.-C. Cyrille, D.-Y. Kim, S.-B. Choe, M. Belmeguenai, M. Hehn, S. Mangin, G. Gaudin and O. Boulle, Appl. Phys. Lett. **112**, 062401 (2018).

[16] J. Finley and L. Liu, Phys. Rev. Appl. **6**, 054001 (2016).

[17] 3K. Garello, I. M. Miron, C. O. Avci, F. Freimuth, Y. Mokrousov, S. Blugel, S. Auffret, O. Boulle, G. Gaudin

and P. Gambardella, Nat. Nanotechnol. **8**, 587 (2013).

[18] W. J. Takei, R. R. Heikes and G. Shirane, Phys. Rev. **125**, 1893 (1962).

[19] Y. Yasutomi, K. Ito, T. Sanai, K. Toko and T. Suemasu, J. Appl. Phys. **115**, 17A935 (2014).

[20] K. Ito, Y. Yasutomi, K. Kabara, T. Gushi, S. Higashikozono, K. Toko, M. Tsunoda and T. Suemasu, AIP Advances **6**, 056201 (2016).

[21] K.-M. Ching, W.-D. Chang and T.-S. Chin, J. Alloys and Compounds **222**, 184 (1995).

[22] K.-M. Ching, W.-D. Chang and T.-S. Chin, Appl. Surf. Sci. **92**, 471 (1996).

[23] S. Nakagawa and M. Naoe, J. Appl. Phys. **75**, 6568 (1994).

[24] S. Dhar, O. Brandt and K. H. Ploog, Appl. Phys. Lett. **86**, 112504 (2005).

[25] X. Shen, A. Chikamatsu, K. Shigematsu, Y. Hirose, T. Fukumura and T. Hasegawa, Appl. Phys. Lett. **105**, 072410 (2014).

[26] K. Kabara and M. Tsunoda, J. Appl. Phys. **117**, 17B512 (2015).

[27] K. Ito, S. Higashikozono, F. Takata, T. Gushi, K. Toko, T. Suemasu, J. Crystal Growth, **455**, 66 (2016).

[28] A. P. Mihai, J. P. Attané, A. Marty, P. Warin and Y. Samson, Phys. Rev. B **77**, 060401(R) (2008).

[29] V. D. Nguyen, L. Vila, P. Laczkowski, A. Marty, T. Faivre and J. P. Attané, Phys. Rev. Lett. **107**, 136605 (2011).

[30] M. Meng, S. X. Wu, L. Z. Ren, W. Q. Zhou, Y. J. Wang, G. L. Wang and S.W. Li, Appl. Phys. Lett. **106**, 032407 (2015).

[31] K. Kabara, M. Tsunoda and S. Kokado, AIP Advances **7**, 056416 (2017).

[32] K. Ito, N. Rougemaille, S. Pizzini, S. Honda, N. Ota, T. Suemasu and O. Fruchart, J. Appl. Phys. **121**, 243904 (2017).

[33] V. Gehanno, Y. Samson, A. Marty, B. Gilles, A. Chamberod, J. Magn. Magn. Mater. 172, 26 (1997).

[34] J. P. Attané, Y. Samson, A. Marty, J. C. Toussaint, G. Dubois, A. Mougin, and J. P. Jamet, Phys. Rev. Lett. **93**, 257203 (2004).

[35] M. Yamanouchi, A. Jander, P. Dhagat, S. Ikeda, F. Matsukura, and H. Ohno, IEEE Magn. Lett., **2**, 3000304 (2011).

[36] F. Ando, H. Kakizakai, T. Koyama, K. Yamada, M. Kawaguchi, S. Kim, K-J. Kim, T. Moriyama, D. Chiba, and T. Ono, Appl. Phys. Lett., **109**, 022401 (2016).

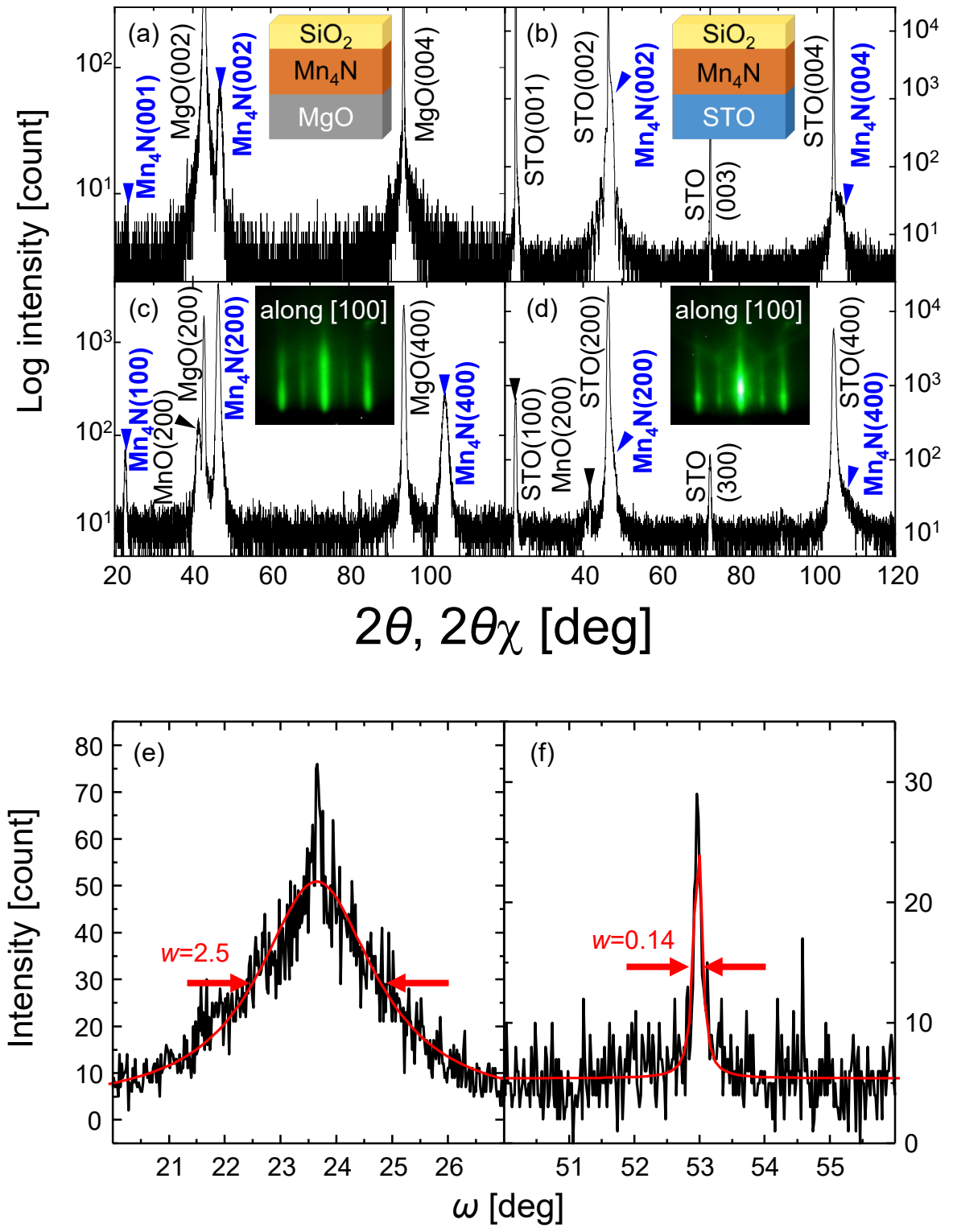

Fig. 1: XRD profiles of Mn_4N films on (a), (c), (e) MgO and (b), (d), (f) STO substrate.
(a), (b) Out-of-plane XRD patterns. Insets show RHEED images of Mn_4N layers taken along the [100] direction of each substrate.
(c), (d) In-plane XRD patterns. The incidence angle and scattering vector were set at ω=0.4° and MgO[200] or STO[200], respectively.
Insets shows each stack structure. Blue marks indicate the peaks attributed to (100)-oriented-Mn_4N.
(e), (f) ω-scan rocking curves for (e) Mn_4N 002 on MgO, and (f) Mn_4N 004 on STO.
Black and red lines present the raw and total fit data with Lorentzian.

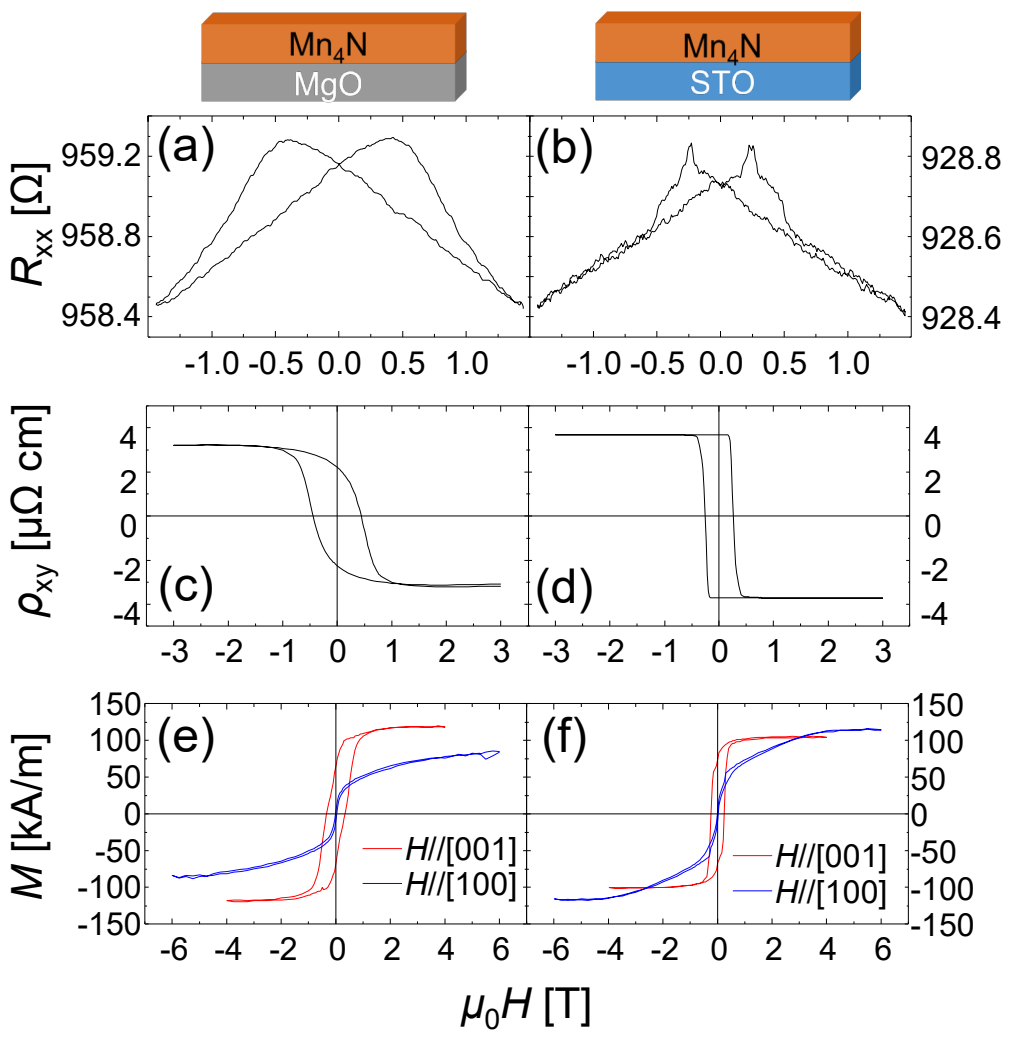

Fig. 2:
(a), (b) Dependence of the longitudinal resistance with the perpendicularly applied magnetic field.
(c), (d) Extraordinary Hall effect hysteresis loops.
(e), (f) Out-of-plane hysteresis loops measured by VSM.
(a), (c), (e) correspond to the Mn_4N/MgO sample, and (b), (d), (f) to the Mn_4N/STO sample.

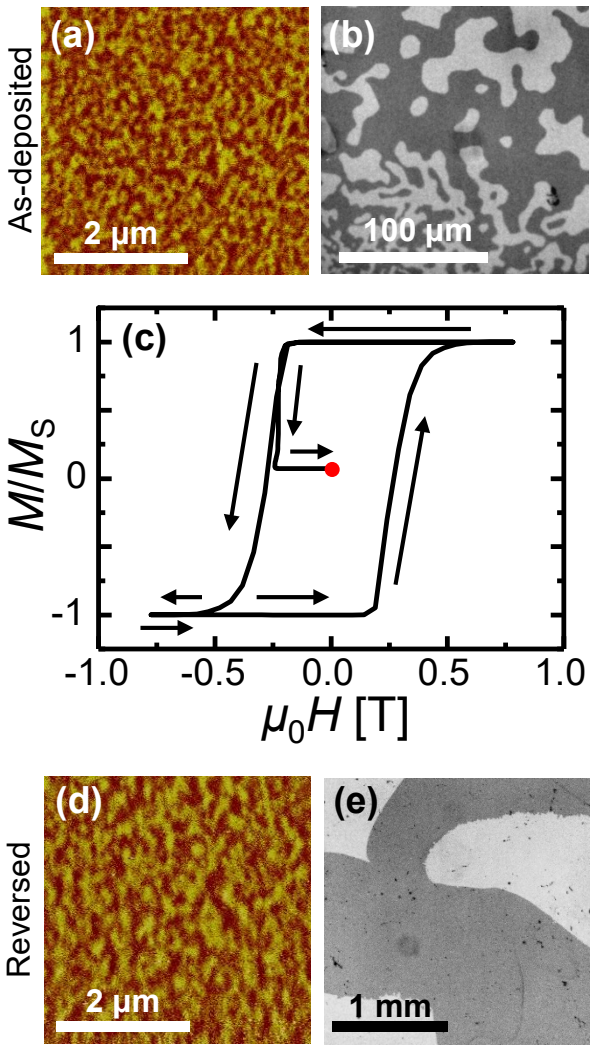

Fig. 3 (a) MFM image of the Mn_4N/MgO and (b) MOKE image of the Mn_4N/STO samples in the as-deposited state.
(c) Magnetization curve illustrating the partial reversal process, monitored by extraordinary Hall effect in the Mn_4N/STO sample. The red dot corresponds to the final magnetization state, used for (e).
(d) MFM image of the Mn_4N/MgO sample and (e) MOKE image of the Mn_4N/STO sample after partial reversal.